Eur. Phys. J. B **51**, 315–319 (2006)
DOI: 10.1140/epjb/e2006-00228-4

THE EUROPEAN PHYSICAL JOURNAL B

O1s and Mn2p NEXAFS on single-layered $La_{1-x}Sr_{1+x}MnO_4$: crystal field effect versus orbital coupling mechanism

M. Merz[1,a], P. Reutler[2], B. Büchner[2], D. Arena[3], J. Dvorak[4], Y.U. Idzerda[4], S. Tokumitsu[5], and S. Schuppler[5]

[1] Institut für Kristallographie, Jägerstraße 17-19, RWTH Aachen, 52066 Aachen, Germany
[2] Institute for Solid State Research, IFW Dresden, P.O. Box 270116, 01171 Dresden, Germany
[3] Naval Research Laboratory, Code 6345, Washington, DC 20375, USA
[4] Department of Physics, Montana State University, Bozeman, MT 59717-3840, USA
[5] Forschungszentrum Karlsruhe, Institut für Festkörperphysik, 76021 Karlsruhe, Germany

Received 20 December 2005 / Received in final form 14 March 2006
Published online 13 June 2006 –

Abstract. O1s and Mn2p near-edge X-ray absorption spectroscopy on $La_{1-x}Sr_{1+x}MnO_4$ ($0 \leq x \leq 0.5$) single crystals shows that Sr doping does not only provide holes to the system but also induces a continuous transfer of electrons from out-of-plane $d_{3z^2-r^2}$ to in-plane $d_{3x^2-r^2}/d_{3y^2-r^2}$ orbitals. Furthermore, a non-vanishing electron occupation of in-plane $d_{x^2-y^2}$ and out-of-plane $d_{3z^2-r^2}$ orbitals is observed up to relatively high doping contents. These findings demonstrate that the energy difference between all these orbital types has to be very small and manifest that the orbital degree of freedom is determined not just by crystal field effects but also by orbital coupling. Moreover, the doping-dependent transfer of spectral weight observed in the current data identifies $La_{1-x}Sr_{1+x}MnO_4$ as a charge-transfer insulator.

PACS. 74.25.Jb Electronic structure – 74.62.Dh Effects of crystal defects, doping and substitution – 78.70.Dm X-ray absorption spectra

1 Introduction

Manganites are, in many respects, peculiar and fascinating transition-metal oxides: beyond the strong electron-correlation effects inherent to many 3d-electron systems, they exhibit cooperative Jahn-Teller interaction, colossal magnetoresistance (CMR), and an unusual interplay between spin, charge, and orbital degrees of freedom. All this leads to a large number of competing magnetic and electronic phases, with charge- and orbital-ordered states being at the center of interest [1]. Among these materials, single-layered $La_{1-x}Sr_{1+x}MnO_4$ stands out: not only does it show, for $x = 0.5$, the same perfect charge/orbital ordering (CO/OO) and CE-type antiferromagnetism usually observed only for its 3D pseudo-cubic perovskite counterparts [2–4] — it does so with a rather 2D character (both structurally and electronically) and without suffering from twinning and multi-domain effects. Undoped $LaSrMnO_4$ ($x = 0.0$) has the body-centered tetragonal K_2NiF_4 structure [5] with O(1) in-plane and O(2) apical oxygen sites. The undoped system is known to be a C-type antiferromagnetic (AFM) insulator below the Néel temperature $T_N \approx 125$ K, yet additional ferromagnetic (FM) correlations are observed in magnetic susceptibility measurements [6]. Hole doping by partial replacement of La^{3+} with Sr^{2+} significantly reduces the resistivity, nevertheless the system remains insulating for all Sr contents x and exhibits CMR only by the application of very high magnetic fields [7]. On the other hand, T_N rapidly decreases with increasing x, and between approximately $0.2 \leq x \leq 0.4$ spin-glass characteristics appear below $T_g \approx 25$ K [2,8]. For $x = 0.5$, finally, the system shows the CO/OO and CE-type phase below $T_{CO/OO} = 225$ K and $T_{CE} = 110$ K, respectively [3]. The e_g orbital ordering in this phase, however, is currently controversial [9–17]: resonant scattering experiments at the Mn K [4,10] and L [14,15] edges point to the generally assumed $d_{3x^2-r^2}/d_{3y^2-r^2}$ pattern, linear dichroism results [16] and more recent resonant scattering experiments at the Mn $L_{II,III}$ edge [17] were interpreted as evidence for the ordering of $d_{z^2-x^2}/d_{z^2-y^2}$ states. Since both ordering scenarios are compatible with the same lattice symmetry it is hard to distinguish between these orbital types, and more direct methods have to be used. To resolve this ambiguity and to determine the room temperature (293 K) e_g orbital occupation in $La_{1-x}Sr_{1+x}MnO_4$ ($0 \leq x \leq 0.5$) we investigated this system with near-edge X-ray absorption fine structure (NEXAFS). O1s and Mn2p NEXAFS probes precisely and sensitively the unoccupied density of states with O2p and Mn3d character, i.e., the relevant states at the Fermi level, E_F. The current study clearly shows that Sr doping does not only

[a] e-mail: merz@xtal.rwth-aachen.de

provide holes to the system but also induces a continuous transfer of electrons from out-of-plane $d_{3z^2-r^2}$ to in-plane $d_{3x^2-r^2}/d_{3y^2-r^2}$ states. Despite the dominant role of these orbitals, a certain electron occupation of the in-plane $d_{x^2-y^2}$ and out-of-plane $d_{3z^2-r^2}$ orbitals is found for the investigated doping range. The current study reveals that the orbital degree of freedom is determined not merely by the crystal field, E_z, but also by an orbital coupling, G, which originates from magnetic, electronic, and/or cooperative Jahn-Teller interactions.

2 NEXAFS on $La_{1-x}Sr_{1+x}MnO_4$

O1s NEXAFS was recorded in bulk-sensitive fluorescence yield (FY), while Mn2p NEXAFS was measured in total electron yield to avoid the strong self-absorption effects present at this edge. The experiments were performed at the National Synchrotron Light Source (NSLS) using the NRL/NSLS beamline U4B, with the energy resolution set to 0.21 (0.29) eV at 530 (640) eV. Simultaneously recorded NiO spectra allow energy calibration to better than 30 meV. Details on crystal growth and data evaluation can be found in [6,18]. The high quality of the single crystals was corroborated by X-ray and neutron diffraction on the same samples [19,20]. These experiments also show that the MnO_6 octahedron has a strong tetragonal distortion $D = d_{Mn-O(1)}/d_{Mn-O(2)} \approx 1.20$ for $x = 0$ [21]. With increasing Sr content, the distortion relaxes and $D = 1.14$, 1.08, 1.06, and 1.03 for $x = 0.13$, 0.25, 0.40, and 0.50, respectively. Using the polarized character of synchrotron radiation for NEXAFS and taking the established picture of the manganites into account where the spectral region around E_F is dominated by O orbitals which are σ-bonded to Mn $3d_{3z^2-r^2}$ and $3d_{x^2-y^2}$ states, $\mathbf{E}\|\mathbf{a}$ (and symmetry-equivalent $\mathbf{E}\|\mathbf{b}$) contributions are mainly caused by unoccupied O(1)$2p_x$ (O(1)$2p_y$) states. By the same token, the O(2)$2p_z$ orbitals of the apical oxygen sites predominantly contribute for $\mathbf{E}\|\mathbf{c}$. Information on the unoccupied Mn3d states can be obtained from the corresponding polarization-dependent NEXAFS of the Mn2p edge, although the situation is more complicated there. Yet hybridizations between O2p_π and Mn t_{2g} orbitals cannot be neglected a priori. Especially for the strongly elongated MnO_6 octahedron of $LaSrMnO_4$, unoccupied $3d_{zx,yz}$ states might be lowered to the energetic position of the $3d_{x^2-y^2}$ states and the corresponding spectral weight could contribute to the NEXAFS spectra. Upon doping, however, the octahedral distortion relaxes, and the spectral weight of the $3d_{zx,yz}$ states should thus be considerably moved to higher energies. The fact that neither for the $\mathbf{E}\|\mathbf{a}$ spectra shown in Figure 1 nor for the $\mathbf{E}\|\mathbf{c}$ spectra depicted in Figure 2, any indication for such a shift is found strongly supports the view that hybridizations between O2p_π and Mn t_{2g} states play only a minor role for the manganites [22]. The corresponding assignment of the $\mathbf{E}\|\mathbf{a}$ and $\mathbf{E}\|\mathbf{c}$ spectral contributions around E_F to O(1)$2p_x$–Mn3$d_{x^2-y^2}$ and O(2)$2p_z$–Mn3$d_{3z^2-r^2}$ hybrid states, respectively, is therefore consistent with the cluster calculations for an MnO_6 octahedron in reference [23].

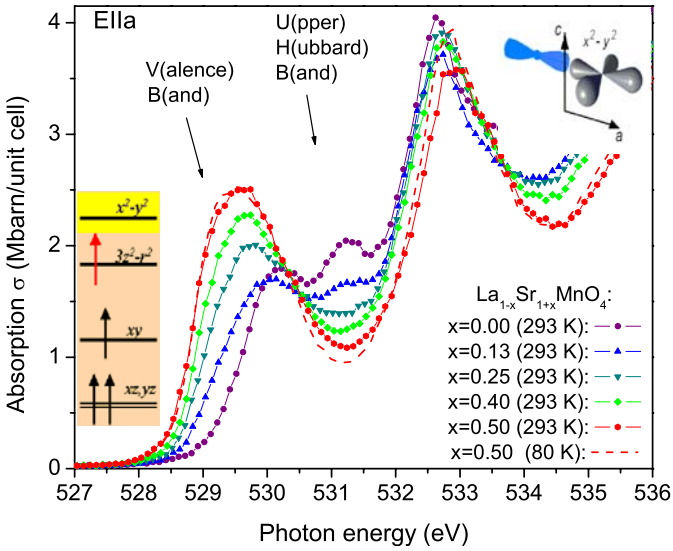

Fig. 1. O1s $\mathbf{E}\|\mathbf{a}$ NEXAFS spectra of $La_{1-x}Sr_{1+x}MnO_4$ ($0 \leq x \leq 0.5$). Upon doping, the spectral weight of the valence band is increased on the expense of the upper Hubbard band. In the left part of the figure the occupation of the e_g and t_{2g} levels expected for are strongly elongated octahedron is depicted. The dashed curve corresponds to the low-temperature ($T = 80$ K) spectrum of $La_{0.5}Sr_{1.5}MnO_4$.

3 Results and discussion

Figure 1 shows the O1s $\mathbf{E}\|\mathbf{a}$ spectra of $La_{1-x}Sr_{1+x}MnO_4$ ($0 \leq x \leq 0.5$) [24]. Three distinct features appear in the spectra: (i) the valence band (VB) whose position moves with doping from ∼530.2 eV to ∼529.5 eV — its spectral weight is a measure for the number of holes in O(1)$2p_x$ (O(1)$2p_y$) orbitals; (ii) the upper Hubbard band (UHB) at ≈531.3 eV — it is seen in O1s spectra due to the σ-type hybridization of the O(1)$2p_x$ (O(1)$2p_y$) orbitals with the Mn3d e_g states. Its intensity is highest when the e_g state is half filled, it disappears when the e_g state is empty, and the doping-dependent transfer of spectral weight observed between this peak and the VB indicates that it can indeed be identified as a UHB; (iii) a pronounced peak at ≈532.7 eV — this feature is attributed to hybridizations with La/Sr states and will not be discussed here in more detail. Additionally, a sketch of the expected occupation of e_g and t_{2g} states for Mn^{3+} in a strongly distorted octahedron is depicted: due to both FM Hund's interaction and strong correlation effects, each of the three t_{2g} levels is singly occupied and the e_g electron is expected to reside in the out-of-plane $d_{3z^2-r^2}$ state while the in-plane $d_{x^2-y^2}$ state remains totally empty.

In accordance with this picture, spectral weight is observed for the VB of undoped $LaSrMnO_4$, i.e., holes reside on O(1)$2p_x$ (O(1)$2p_y$) orbitals which are strongly hybridized with $d_{x^2-y^2}$ states. Simultaneously, however, also a remarkable intensity of the UHB is observed for undoped $LaSrMnO_4$. This, in turn, means that the in-plane $d_{x^2-y^2}$ states are not completely empty and since in total only one electron remains for the two e_g orbitals, some extra

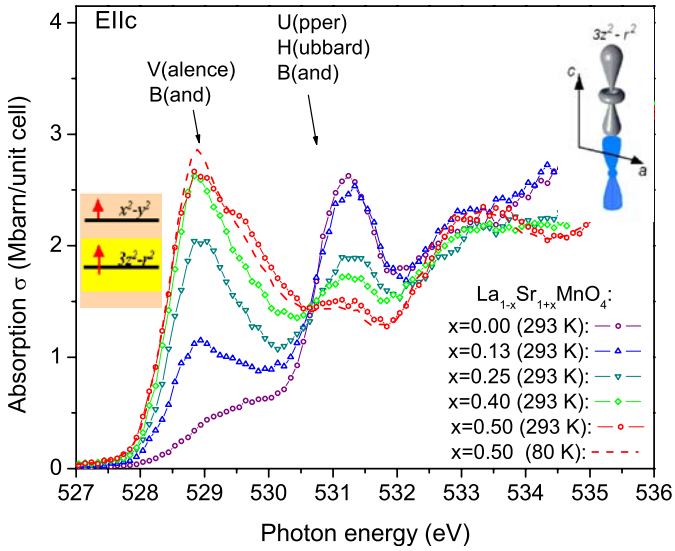

Fig. 2. O1s **E**$\|$**c** NEXAFS spectra of $La_{1-x}Sr_{1+x}MnO_4$ ($0 \leq x \leq 0.5$). Upon doping, the VB is increased, the UHB reduced. For $x = 0.5$ a clear double-peak feature occurs. In the left part a sketch of the experimentally observed electron distribution on the e_g levels is given. The dashed curve corresponds to the low-temperature ($T = 80$ K) spectrum of $La_{0.5}Sr_{1.5}MnO_4$.

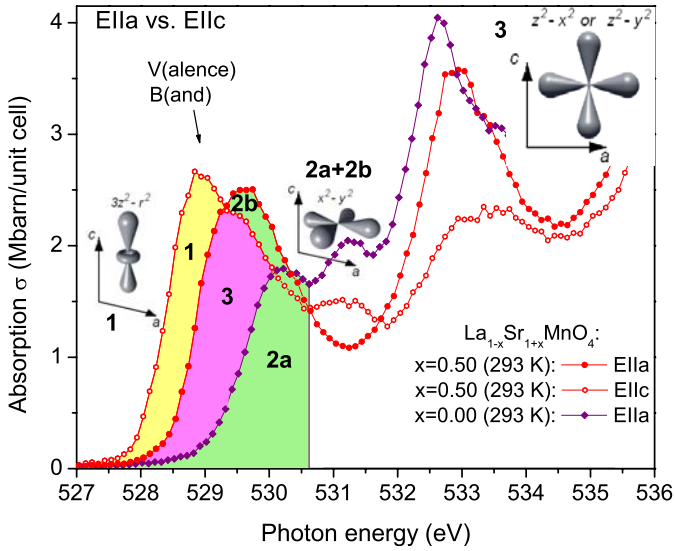

Fig. 3. Comparison of O1s **E**$\|$**a** and **E**$\|$**c** spectra of $La_{0.5}Sr_{1.5}MnO_4$ with **E**$\|$**a** data of $LaSrMnO_4$. The spectral range between 527 and 530.5 eV is divided into four areas for oxygen hybridizations with: **1** $d_{3z^2-r^2}$, **2a** and **2b** $d_{x^2-y^2}$, and **3** $d_{z^2-x^2}/d_{z^2-y^2}$ states.

holes have to reside on out-of-plane $d_{3z^2-r^2}$ states, moving this band away from half filling.

Confirmation for this view comes from the corresponding O1s **E**$\|$**c** spectra of $LaSrMnO_4$ in Figure 2. There, a distinct UHB is observed which points to a high (yet less than half-filled) electron occupation of the $d_{3z^2-r^2}$ states. Nevertheless, a noticeable VB feature appears, indicating that a certain amount of holes occupies out-of-plane $d_{3z^2-r^2}$ and a complementing small number of electrons in-plane $d_{x^2-y^2}$ states. Rough estimates for the hole/electron count derived from an orbital-dependent integration [25] point to an electron occupation of ≈15% (0.15 electrons) for the $d_{x^2-y^2}$ orbitals. Upon increasing the Sr content x, the spectral changes observed in Figures 1 and 2 show the typical charge-transfer insulator behavior: the UHB is continuously reduced and the VB increases, indicating that holes are created in in-plane and out-of-plane states and that spectral weight is transferred from the UHB to the VB. At first glance, this might seem to mean as if further electrons were to be removed from already empty $d_{x^2-y^2}$ states. Of course, this is not the case, and this point will be clarified below. In contrast to the **E**$\|$**a** data, where the UHB is suppressed for the higher doping contents, a clear UHB feature persists for all Sr concentrations in the **E**$\|$**c** spectra, i.e., a decreasing but non-vanishing number of electrons is present in $d_{3z^2-r^2}$ states for the investigated doping range. For $La_{0.5}Sr_{1.5}MnO_4$, finally, the **E**$\|$**c** data of Figure 2 exhibit a marked VB double-peak structure (for which first indications might be conjectured already for samples with lower Sr content). This shows that the O(2)2p_z orbitals are hybridized not only to $d_{3z^2-r^2}$ states but also to another type of Mn3d states with apparent out-of-plane contributions. In order to identify these states and to obtain some crude estimates for the orbital occupations, we compare in Figure 3 the **E**$\|$**a** and **E**$\|$**c** spectra of $La_{0.5}Sr_{1.5}MnO_4$ with the **E**$\|$**a** data of $LaSrMnO_4$. With the conspicuous double-peak feature present, the spectral range between 527 and 530.5 eV should roughly be divided into four regions: Area 1 (yellow) only appears for the **E**$\|$**c** data of $La_{0.5}Sr_{1.5}MnO_4$ and, hence, can easily be assigned to O(2)2p_z orbitals hybridized with $d_{3z^2-r^2}$ states. Area 2a (green) was already discussed above and is ascribed to O(1)2p_x (O(1)2p_y) orbitals hybridized with $d_{x^2-y^2}$ states. Area 2b (green) occurs just for the **E**$\|$**a** spectra of $La_{0.5}Sr_{1.5}MnO_4$ and, thus, is attributed to the same hybrid states. Area 3 (magenta) contains the remaining spectral weight. Since this intensity shows up in both the **E**$\|$**a** (**E**$\|$**b**) and the **E**$\|$**c** spectra of $La_{0.5}Sr_{1.5}MnO_4$, it has to belong to hybrid states which are σ-bonded to O(1,2)2p orbitals and are symmetric with respect to the x- (y-) and z-axis. The only states fulfilling these criteria are the $d_{z^2-x^2}$ ($d_{z^2-y^2}$) states. Hence, the aforementioned doping-dependent increase of the VB in the **E**$\|$**a** spectra of Figure 1 is not caused by a decrease of electrons on $d_{x^2-y^2}$ states but rather by an increase of holes on $d_{z^2-x^2}$ ($d_{z^2-y^2}$) orbitals.

Upon cooling $La_{0.5}Sr_{1.5}MnO_4$ down to 80 K, only small spectral changes are observed (dashed lines in Figs. 1 and 2), and in the terminology of Figure 3, the out-of-plane spectra of Figure 2 suggest a slight increase of Area 1 at the expense of Area 3. If anything, such a finding would not be compatible with simply a reduced phonon broadening [26] but points to a certain, small transfer of holes between $d_{3z^2-r^2}$ and $d_{z^2-x^2}$ ($d_{z^2-y^2}$) states with temperature. That the transfer is but small, on the other hand, directly shows that even at RT most of the e_g electrons

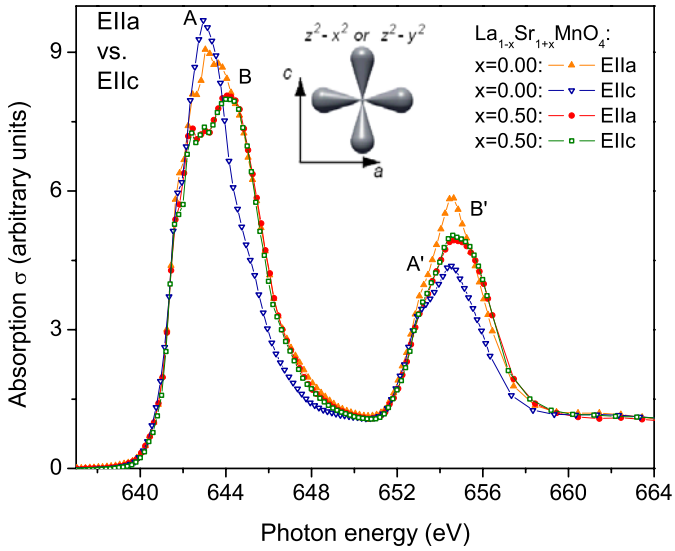

Fig. 4. Comparison of the Mn$L_{\mathrm{II,III}}$ **E**$\|$**a** and **E**$\|$**c** spectra of $LaSrMnO_4$ and $La_{0.5}Sr_{1.5}MnO_4$ taken at 293 K. While for $LaSrMnO_4$ the in-plane and out-of-plane spectra strongly differ, they are almost identical for $La_{0.5}Sr_{1.5}MnO_4$. This implies that for the latter, holes reside on hybrid states which are symmetric along the x- (y-) and z-axis.

already do reside on in-plane ($d_{3x^2-r^2}/d_{3y^2-r^2}$) orbitals. Diffraction [19,20] and soft X-ray resonant scattering experiments [27] indicate an additional in-plane distortion of the Mn-O(1) bond for $T \leq T_{\mathrm{CO/OO}} \sim 225$ K, which, in turn, suggests that for lower temperature the in-plane e_g electrons become increasingly localized since the $d_{3x^2-r^2}$ and $d_{3y^2-r^2}$ orbitals start to arrange themselves according to the CE-type charge and orbital ordering pattern. The present data show that this occurs without any further significant transfer of electrons to the in-plane orbitals, let alone a change in the orbital character.

The O1s results must be reflected at the Mn2p edge as well. In Figure 4 the Mn2p **E**$\|$**a** and **E**$\|$**c** spectra, normalized at 670 eV, are shown for undoped $LaSrMnO_4$ and half-doped $La_{0.5}Sr_{1.5}MnO_4$. Corresponding to the 6 (7) holes expected for a Mn^{3+} $3d^4$ (Mn^{4+} $3d^3$) configuration the L_{III} and the L_{II} edge have a high intensity and a width of ~4 eV. Obviously, the **E**$\|$**a** and **E**$\|$**c** spectra of $LaSrMnO_4$ strongly differ from each other, i.e., holes/electrons reside on different orbitals [24]. With increasing hole content x, the **E**$\|$**a** intensity of the L_{III} (L_{II}) edge is considerably reduced and for **E**$\|$**c** spectral weight is redistributed between feature **A** (**A**′) and **B** (**B**′) at the L_{III} (L_{II}) edge. The intensity reduction observed for **E**$\|$**a** despite of an increasing hole content clearly indicates that hole doping induces a transfer of electrons from out-of-plane states to orbitals with noticeable in-plane contributions. The **E**$\|$**c** data show that spectral weight is redistributed until for $La_{0.5}Sr_{1.5}MnO_4$ the **E**$\|$**a** and **E**$\|$**c** spectra are almost point-to-point equivalent, illustrating that for $x = 0.5$ holes reside on hybrid states which are symmetric with respect to the x- (y-) and z-axis. Thus, the Mn2p spectra support the result of the O1s data that for $x = 0.5$ holes mainly reside on $d_{z^2-x^2}/d_{z^2-y^2}$ states and, consequently, electrons predominantly occupy the corresponding orthogonal states, i.e., $d_{3x^2-r^2}/d_{3y^2-r^2}$ orbitals.

For $La_{0.5}Sr_{1.5}MnO_4$, a crude estimate (similar to the one above for $LaSrMnO_4$) derived from the O1s edge indicates an electron occupation of ≈85% (0.42 electrons) for the $d_{3x^2-r^2}/d_{3y^2-r^2}$ hybrids while ≈15% (0.08 electrons) remain on the $d_{3z^2-r^2}$ hybrids. This is at variance with the interpretation in reference [16], and already the Mn2p linear dichroism derived from the present data points to a simultaneous occupation of $d_{3x^2-r^2}$, $d_{3y^2-r^2}$, and $d_{3z^2-r^2}$ hybrids.

4 Conclusions

In summary, the following picture can be assembled from the NEXAFS results: For the strong tetragonal distortion of the octahedra in undoped $LaSrMnO_4$, the crystal field establishes an AFM ferrodistortive ordering and electrons mainly occupy out-of-plane O(2)2p_z-Mn3$d_{3z^2-r^2}$ and holes in-plane O(1)2$p_{x,y}$-Mn3$d_{x^2-y^2}$ states. Contrary to what is widely believed, however, the former are not completely filled and the latter not totally empty. This is possible only when the energy difference of these orbitals is much smaller than expected from mere crystal field splitting. In other words, E_{z} seems to be almost — yet not fully — compensated by an antiferrodistortive coupling, G, originating from magnetic, electronic or cooperative Jahn-Teller interactions [28], and $E_{\mathrm{z}} \gtrsim G$. Nevertheless, NEXAFS cannot decide if electrons on the Mn^{3+} sites fluctuate between these orbitals or if the occupation of the $d_{x^2-y^2}$ states is energetically favored on specific octahedra. Phase separation into domains with a size of several μm, however, where either the $d_{x^2-y^2}$ or the $d_{3z^2-r^2}$ orbitals are favored on all Mn sites can be excluded from our X-ray diffraction investigations [19]. In any case, the fact that electrons reside in $d_{x^2-y^2}$ states as well explains the additional ferromagnetic (FM) correlations seen in susceptibility measurements [6] on the same samples. With increasing Sr content, the cooperative coupling starts to compensate the crystal field splitting fully ($E_{\mathrm{z}} \approx G$) and electrons are continuously transferred to in-plane $d_{3x^2-r^2}/d_{3y^2-r^2}$ orbitals. The almost degenerate energies for the $d_{3x^2-r^2}/d_{3y^2-r^2}$ and $d_{3z^2-r^2}$ orbitals also lead to a high degree of orbital disorder which is reflected by the large temperature factors observed in diffraction data on the same crystals [19,20] and by the spin-glass behavior for samples with $0.2 \leq x \leq 0.4$ [2,8]. For $La_{0.5}Sr_{1.5}MnO_4$, finally, the checkerboard arrangement of valence-ordered Mn^{3+} and Mn^{4+} with electrons on alternating $d_{3x^2-r^2}$ and $d_{3y^2-r^2}$ orbitals at Mn^{3+} sites is expected from diffraction data at $T \leq 225$ K. Even in this doping regime, however, the present NEXAFS results indicate a temperature-independent non-vanishing amount of electrons remaining on out-of-plane $d_{3z^2-r^2}$ states. On-site correlation effects produced by these electrons may also explain why $La_{0.5}Sr_{1.5}MnO_4$ is an insulator instead of a one-dimensional metal which might be expected from the Zener double-exchange for neighboring

Mn^{3+}/Mn^{4+} sites [29]. Since also for $x = 0.5$ a temperature-independent tetragonal distortion of ≈3% persists for the octahedra, it is $0 < E_z \lesssim G$. In all instances, thus, orbital coupling seems to be the driving force for the electron occupation of in-plane $d_{3x^2-r^2}/d_{3y^2-r^2}$ states, while the crystal field is responsible for the electrons remaining in the out-of-plane $d_{3z^2-r^2}$ orbitals. This result again shows that the orbital degree of freedom in single-layered $La_{1-x}Sr_{1+x}MnO_4$ ($0 \le x \le 0.5$) is determined by a delicate balance between crystal field effects and orbital coupling mechanisms provoked by magnetic, electronic and/or cooperative Jahn-Teller interactions. In effect, this fine balance then leads to almost degenerate energies for the $d_{x^2-y^2}$, $d_{3z^2-r^2}$, and $d_{3x^2-r^2}/d_{3y^2-r^2}$ orbitals.

We greatly appreciate experimental help by and fruitful discussions with M. Braden, G. Heger, S.L. Hulbert, D. Khomskii, P. Nagel, G. Nintzel, and G. Roth. Research was carried out in part at the National Synchrotron Light Source, Brookhaven National Laboratory, which is supported by the U.S. Department of Energy, Division of Material Sciences and Division of Chemical Sciences.

References

1. Y. Tokura, N. Nagosa, Science **288**, 462 (2000)
2. Y. Moritomo, Y. Tomioka, A. Asamitsu, Y. Tokura, Y. Matsui, Phys. Rev. B **51**, 3297 (1995)
3. B.J. Sternlieb, J.P. Hill, U.C. Wildgruber, G.M. Luke, B. Nachumi, Y. Moritomo, Y. Tokura, Phys. Rev. Lett. **76**, 2169 (1996)
4. Y. Murakami, H. Kawada, H. Kawata, M. Tanaka, T. Arima, Y. Moritomo, Y. Tokura, Phys. Rev. Lett. **80**, 1932 (1998)
5. J.-C. Bouloux, J.-L. Soubeyroux, A. Daoudi, G. Leflem, Mat. Res. Bull. **16**, 855 (1981)
6. P. Reutler, O. Friedt, B. Büchner, M. Braden, A. Revcolevschi, J. Cryst. Growth **249**, 222 (2003); P. Reutler, Ph.D. thesis
7. M. Tokunaga, N. Miura, Y. Moritomo, Y. Tokura, Phys. Rev. B **59**, 11151 (1999)
8. C. Baumann, G. Allodi, B. Büchner, R. De Renzi, P. Reutler, A. Revcolevschi, Physica B **326**, 505 (2003)
9. S. Larochelle, A. Mehta, N. Kaneko, P.K. Mang, A.F. Panchula, L. Zhou, J. Arthur, M. Greven, Phys. Rev. Lett. **87**, 095502 (2001)
10. Y. Murakami, J.P. Hill, D. Gibbs, M. Blume, I. Koyama, M. Tanaka, H. Kawata, T. Arima, Y. Tokura, K. Hirota, Y. Endoh, Phys. Rev. Lett. **81**, 582 (1998)
11. S. Ishihara, S. Maekawa, Phys. Rev. Lett. **80**, 3799 (1998)
12. M. Benfatto, Y. Joly, C.R. Natoli, Phys. Rev. Lett. **83**, 636 (1999)
13. I.S. Elfimov, V.I. Anisimov, G.A. Sawatzky, Phys. Rev. Lett. **82**, 4264 (1999)
14. S.B. Wilkins, P.D. Spencer, P.D. Hatton, S.P. Collins, M.D. Roper, D. Prabhakaran, A.T. Boothroyd, Phys. Rev. Lett. **91**, 167205 (2003)
15. S.S. Dhesi, A. Mirone, C. De Nadaï, P. Ohresser, P. Bencok, N.B. Brookes, P. Reutler, A. Revcolevschi, A. Tagliaferri, O. Toulemonde, G. van der Laan, Phys. Rev. Lett. **92**, 056403 (2004)
16. D.J. Huang, W.B. Wu, G.Y. Guo, H.-J. Lin, T.Y. Hou, C.F. Chang, C.T. Chen, A. Fujimori, T. Kimura, H.B. Huang, A. Tanaka, T. Jo, Phys. Rev. Lett. **92**, 087202 (2004)
17. S.B. Wilkins, N. Stojić, T.A.W. Beale, N. Binggeli, C.W.M. Castleton, P. Bencok, D. Prabhakaran, A.T. Boothroyd, P.D. Hatton, M. Altarelli, Phys. Rev. B **71**, 245102 (2005)
18. M. Merz, N. Nücker, E. Pellegrin, P. Schweiss, S. Schuppler, M. Kielwein, M. Knupfer, M.S. Golden, J. Fink, C.T. Chen, V. Chakarian, Y.U. Idzerda, A. Erb, Phys. Rev. B **55**, 9160 (1997); M. Merz, N. Nücker, P. Schweiss, S. Schuppler, C.T. Chen, V. Chakarian, J. Freeland, Y.U. Idzerda, M. Kläser, G. Müller-Vogt, Th. Wolf, Phys. Rev. Lett. **80**, 5192 (1998)
19. M. Merz, to be submitted
20. D. Senff, P. Reutler, M. Braden, O. Friedt, D. Bruns, A. Cousson, F. Bourée, M. Merz, B. Büchner, A. Revcolevschi, Phys. Rev. B **71**, 024425 (2005); in this article the nominal Sr content of our $x = 0.13$ sample was determined to 0.125
21. In reference [20], the doping- and temperature-dependent changes of the Mn-O(1) and Mn-O(2) bond lenghts and of the thermal expansion were interpreted in terms of the orbital degree of freedom. Bond distances, however, are only an indirect measure of orbital occupations as seen, e.g., for isostructural $LaSrAlO_4$ where an elongated octahedron appears even though the Al^{3+} ion is not Jahn-Teller active
22. Nevertheless, such hybridizations may lead to a small background with doping-independent intensity in the spectra.
23. J. van Elp, A. Tanaka, Phys. Rev. B **60**, 5331 (1999)
24. The symmetry-equivalent $\mathbf{E}\|\mathbf{a}$ and $\mathbf{E}\|\mathbf{b}$ spectra are identical within the experimental error and, thus, the $\mathbf{E}\|\mathbf{b}$ data are left out for clarity
25. Details on the integration method for obtaining hole counts are given in reference [18]
26. F.M.F. de Groot, J.C. Fuggle, B.T. Thole, G.A. Sawatzky, Phys. Rev. B **41**, 928 (1990)
27. U. Staub, V. Scagnoli, A.M. Mulders, K. Katsumata, Z. Honda, H. Grimmer, M. Horisberger, J.M. Tonnerre, Phys. Rev. B **71**, 214421 (2005)
28. D.I. Khomskii, K.I. Kugel, Phys. Rev. B **67**, 134401 (2003)
29. J. van den Brink, G. Khaliullin, D.I. Khomskii, Phys. Rev. Lett. **83**, 5118 (1999)